

Quantum Advantage for Integral Transforms

Doğa Veske^{*1,2}, Cenk Tüysüz^{3,4}, Mirko Amico⁵, Nicholas T. Bronn⁵, Olivia T. Lanes⁵,
Imre Bartos⁶, Zsuzsa Márka⁷, Sebastian Will¹, and Szabolcs Márka¹

¹Department of Physics, Columbia University in the City of New York, New York, NY, 10027, USA

²Institute for Theoretical Physics, Heidelberg University, Heidelberg, 69120, Germany

³Deutsches Elektronen-Synchrotron DESY, Platanenallee 6, Zeuthen, 15738, Germany

⁴Institut für Physik, Humboldt-Universität zu Berlin, Newtonstr. 15, Berlin, 12489, Germany

⁵IBM Quantum, IBM T.J. Watson Research Center, Yorktown Heights, NY, USA

⁶Department of Physics, University of Florida, Gainesville, FL, 32611-8440, USA

⁷Columbia Astrophysics Laboratory, Columbia University in the City of New York, New York, NY, 10027, USA

Abstract

Quantum computers promise to revolutionize some of the most computationally challenging tasks by executing calculations faster than classical computers. Integral transforms, such as convolution, Laplace transform, or path integration in quantum mechanics, are indispensable operations of scientific and technological progress. They are used from solving integro-differential equations to system modeling and signal processing. With the rapidly growing amount of collected information and the development of more complex systems, faster computations of integral transforms could dramatically expand analysis, design and execution capabilities. Here we show that the use of quantum processors can reduce the time complexity of integral transform evaluations from quadratic to quasi-linear. We present an experimental demonstration of the quantum-enhanced strategy for matched filtering. We implemented the qubit-based matched filtering algorithm on noisy superconducting qubits to carry out the first quantum-based gravitational-wave data analysis. We obtained a signal-to-noise ratio with this analysis for a binary black hole merger similar to that achievable with classical

computation, providing evidence for the utility of qubits for practically relevant tasks. The presented algorithm is generally applicable to any integral transform with any number of integrands in any dimensions.

1 Introduction

Since ancient times, harmonic series have been in use for calculating the trajectories of astronomical objects [1]. In the 19th century, Fourier's theory was firmly established for representing any function with a sum of complex exponentials [2, 3]. The Fourier transform has been used extensively from its original use to solve the heat equation to its virtually ubiquitous use today in signal processing. Being calculated with the help of a sum or integral, the Fourier transform is a type of integral transform. Today, the use of integral transforms is not only limited to Fourier transform; but they are used in many areas [4]; for example in modeling the system or filter responses [5], calculating the insolvency probabilities of insurers with ruin theory [6], sonars, reconstruction of the tomograms, convolutional neural networks and calculating the correlation functions in quantum field theories [7, 8]. In

^{*}veske@thphys.uni-heidelberg.de

general, their digitized versions involve sums of the form

$$\rho[j] = \sum_{i=1}^N x[i, j]y[j - i], \quad j = 1, 2, \dots, L \quad (1)$$

where the function y is transformed to ρ with the help of the kernel (or the impulse response) x . Considering a specific example of a linear system for concreteness; i and j can be indices representing time, y can be an input of length L , x the impulse response of length N and ρ the output. The computational cost of this calculation is proportional to the length of the data and the filter's impulse response, i.e. $\mathcal{O}(NL)$. In the special case of a time independent impulse response, i.e. $x[i, j] = x[i]$, the output ρ can be calculated efficiently in frequency domain using fast Fourier transform (FFT) with $\mathcal{O}(L \log N)$ time complexity. However, in the general case the $\mathcal{O}(NL)$ scaling remains for classical computers and limits the computational feasibility of integral transforms. Examples for time variant systems span from modeling periodic natural phenomena, such as response of the atmosphere with daily or annual periodicity, to artificial applications such as speech synthesis [9].

Here, we introduce and experimentally demonstrate an algorithm that uses quantum circuits together with classical operations to compute sums of the form Eq. (1) quasi-quadratically faster than a classical computer for real valued functions; its time complexity scales as $\mathcal{O}(L(\log N)^2)$. The algorithm, and its experimental implementation we present below, provides evidence for the advantageous use of quantum computers for practically useful tasks, which have not been specifically crafted and demonstrated for quantum computers. In the presented algorithm, the only quantum operations we perform are encoding of the problem into a string of qubits and performing quantum measurements on them. These operations, without additional quantum computation can, by themselves, provide a quantum advantage as we explain below.

Quantum encoding and measurement can generate random bitstrings according to a probability distribution exponentially faster than classical generation. We basically exploit this attribute. This *shallow* use of quantum bits makes our method more robust against the noise of the quantum hard-

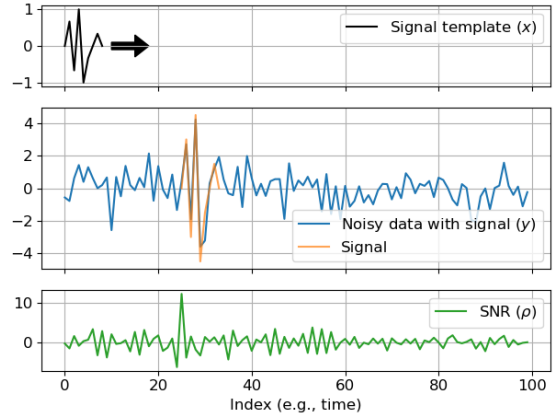


Figure 1: An example illustration of matched filtering. Noisy data (blue) which contains a signal (orange) embedded in white Gaussian noise is shown. The SNR series (green) is found by shifting the signal template (black) through the data and finding the inner product of it with the overlapping data segment as in Eq. (2). The obtained SNR series shows a clear peak around index 25 where the signal was located.

ware without any error correction. This is the main reason why we were able to demonstrate our method on real quantum hardware with high accuracy.

Without the loss of generality, we demonstrated our algorithm on matched filtering, which is the optimal system for searching for a known signal template buried in Gaussian noise [10]. Originally developed for detecting radar echoes in the 1950's [11], thanks to its approximate optimality for many real world applications, it is now used in many different areas from gravitational-wave detection [12, 13] to quantum tomography via correlation of noisy measurements [14]. For a known digitized template signal x_i with N points and data stream y_i with L points ($N \leq L$) in the presence of white noise, in time domain, the signal-to-noise ratio (SNR) of a matched filter can be calculated with a convolution as

$$\rho[j] = \sum_{i=1}^N y_{i+j}x_i \quad (2)$$

This is illustrated in Fig. 1. In the presence of colored noise, x and y additionally need to be nor-

malized using the noise's power spectral density. For our demonstration, we chose matched filtering, which is a time-independent system; besides its wide use, mainly due to the limited number of qubits we could use. With the current qubit technology, implementing significantly more information about a time-dependent system was not feasible. As we explain next, we do not use any mathematical symmetry of complex exponentials, which are the basis for FFT and makes this calculation classically faster. The improvement in our algorithm comes from the qubits for the most general scenario, unlike FFT's benefit only for time-independent systems. Our solution can be seen as a Monte Carlo solution where the qubits can sample the parameter space exponentially faster.

2 Method

The main advantage in our method comes from the fact that it works only with real valued signals for which no phases beyond their signs exist. That allows us to use measurements more effectively where the phase information is lost. We were inspired by combining quantum and classical logic operations by Ref. [15], in which similar approaches were discovered for equivalent constructions of swap test with the purpose of simplifying the original quantum circuit of the swap test with classical additions. Before moving on to our method, we also mention that another possible way of doing this calculation with quantum computing than our method is via a swap test, which calculates the overlap of two states $=|\langle\phi|\psi\rangle|^2$. However, we could not find a way of employing it with a time complexity improvement over the classical computation. The main bottleneck seemed to be the computation for the design of encoding circuits.

To illustrate the improvement in the computation capability with our method, first assume the values of the vectors we want to have their convolution are positive and consider the square roots of the values are encoded with amplitude encoding.

$$\text{Data} = |y\rangle = \mathcal{N}_y^{-1} \sum_{i=1}^L \sqrt{y_i} |i\rangle_y, \quad (3a)$$

$$\text{Signal} = |x\rangle = \mathcal{N}_x^{-1} \sum_{i=1}^N \sqrt{x_i} |i\rangle_x \quad (3b)$$

where $|i\rangle$ are the 2^n possible basis states obtainable with n qubits, i.e. $|00\rangle, |01\rangle, |10\rangle, |11\rangle$ for 2 qubits. $\mathcal{N}_x = \sum_{i=1}^N x_i$ and $\mathcal{N}_y = \sum_{i=1}^L y_i$ are the normalizations

The overall state with the encoded data and the signal is

$$|\psi\rangle = \mathcal{N}_y^{-1} \mathcal{N}_x^{-1} \sum_{i=1}^N \sum_{j=1}^L \sqrt{y_j} \sqrt{x_i} |j\rangle_y |i\rangle_x \quad (4)$$

Now the SNR for a signal starting at the data point j can be computed by obtaining the result

$$\begin{aligned} \rho(j) &= \mathcal{N}_y \mathcal{N}_x \sum_{i=1}^N |\langle i+j|_y \langle i|_x |\psi\rangle|^2 \\ &= \sum_{i=1}^N |\sqrt{y_{i+j}} \sqrt{x_i}|^2 = \sum_{i=1}^N y_{i+j} x_i \end{aligned} \quad (5)$$

So adding up the probabilities of measuring the state $|i+j\rangle_d |i\rangle_s$ for the encoded qubits over all the values of i and for a fixed j value gives the SNR for a search at point j (up to the normalization constants). Moreover, this addition is not needed to be done after probability of each combination is calculated; because when we make a measurement on the qubits, any possible outcome may be measured, which gives information for one of the possible j values. Therefore each repetition of this procedure contains information about all of the j values since the probability of any of them appearing is dependent on the encoded information. Thus, after the measurements, a parallelized logic circuit can be constructed whose inputs are the measurement results of the qubit states and which gives binary 1 for the states which are wanted to be add up and 0 otherwise for each j value. For example, for a 2 point signal and 2 point data, there is only one meaningful SNR to be calculated: $x_0 y_0 + x_1 y_1$. This corresponds to estimating the probability of finding the qubits in the states $|0\rangle_x |0\rangle_y$ or $|1\rangle_x |1\rangle_y$. So the expectation value of $\text{XNOR}(q_y, q_x)$ can be directly estimated rather than first estimating $P(|0\rangle_x |0\rangle_y)$ and $P(|1\rangle_x |1\rangle_y)$ and then adding up. For a general integral transform, there are going to be total of $\log_2 NL^2$ qubits to be measured and NL^2 possible different outcomes. SNR of each data point j is proportional to the number of measurements of mutually exclusive

NL of these possible different outcomes. Therefore depth of the logic circuits constructed with OR gates with 2 inputs are $\mathcal{O}(\log_2 NL)$. The expansion of $\log_2 NL^2$ qubits to NL^2 different logic functions can be done with 2 input AND gates and inverters with depth $\mathcal{O}(\log \log NL^2)$. Total number of needed AND gates and inverters, without any logical simplifications, e.g. with a Karnaugh map [16]; will be $\mathcal{O}(L \log NL^2)$ and OR gates will be $\mathcal{O}(NL^2)$. In this description we used the fact that any logic function can be written as sums (OR) of products (AND) of its variables and the inverted variables.

The computation time in this case becomes

$$T[\text{Encoding time} + \text{Measurement time} + \mathcal{O}(\log(NL \log NL^2)) \times \text{propagation time for logic gates}] \quad (6)$$

where T is the number of measurements (shots) for achieving a necessary precision. For a fixed precision, T scales with L since each measurement outcome is distributed to one of the L possible times. Measurements on qubits can be done simultaneously so, the measurement time per shot is constant. The divide and conquer algorithm mentioned [17] does the amplitude encoding for n point signal with a circuit with depth $\mathcal{O}((\log n)^2)$ and with width (total necessary qubit count) $\mathcal{O}(n)$. Hence, the encoding time dominates the expression in the parentheses and the total time complexity becomes $\mathcal{O}(L(\log L)^2)$. There are two other computation times in hindsight which are the design of the encoding circuit for data which is done once per application and has time complexity $\mathcal{O}(L)$ and the square rooting the original values of data whose time complexity is also $\mathcal{O}(L)$. These do not affect the asymptotic behaviour of $\mathcal{O}(L(\log L)^2)$. We ignore such costs for the template, which are $\mathcal{O}(NL)$ for a time dependent one; as for a widely used one, these can be calculated once and can be used directly for different data, like a function in a software library. Compared to the classical computation's time complexity $\mathcal{O}(NL)$, this method improves the computation time for long kernels $N \gg (\log L)^2$.

The description above works only for the positive values since we need to encode the square roots of the values. Solution to the negative numbers is to shift the data and signal by the magnitude of their minimum negative value so that all the numbers

become positive.

$$\text{Data} = |y\rangle = \mathcal{N}_y^{-1} \sum_{i=1}^L \sqrt{y_i + \Delta y} |i\rangle_y, \quad (7a)$$

$$\text{Signal} = |x\rangle = \mathcal{N}_x^{-1} \sum_{i=1}^N \sqrt{x_i + \Delta x} |i\rangle_x \quad (7b)$$

where $\Delta x = -\min(x_i)$ and $\Delta y = -\min(y_i)$, with new normalizations $\mathcal{N}_x = \sum_{i=1}^N (x_i + \Delta x)$ and $\mathcal{N}_y = \sum_{i=1}^L (y_i + \Delta y)$.

Of course, this effect needs to be corrected later when calculating SNR since

$$\begin{aligned} \mathcal{N}_y \mathcal{N}_x \sum_{i=1}^N |\langle i + j |_y \langle i |_x | \psi \rangle|^2 \\ = \sum_{i=1}^N |\sqrt{y_{i+j} + \Delta y} \sqrt{x_i + \Delta x}|^2 \\ = \sum_{i=1}^N y_{i+j} x_i + \Delta y x_i + \Delta x y_{i+j} + \Delta y \Delta x \end{aligned} \quad (8)$$

The necessary correction is subtracting the extra terms as

$$\begin{aligned} \rho(j) = \mathcal{N}_y \mathcal{N}_x \sum_{i=1}^N |\langle i + j |_y \langle i |_x | \psi \rangle|^2 \\ - \sum_{i=1}^N \Delta y x_i + \Delta x y_{i+j} + \Delta y \Delta x \end{aligned} \quad (9)$$

In this correction only the $\sum_{i=1}^N \Delta x y_{i+j}$ term is not a constant term. Although it seems that N additions need to be made for calculating it for every L values of j , since the difference between the consecutive values of the correction is just 2 numbers (first number of the previous step and the last number of the new step), asymptotically $\mathcal{O}(N + L)$ operations are needed for calculating every L value of it. Hence, addition of this correction does not affect the previous scaling which was $\mathcal{O}(L(\log L)^2)$.

Since the overall scaling $\mathcal{O}(L(\log L)^2)$ grows faster than linear scaling $\mathcal{O}(L)$, one might suggest to divide the data into smaller segments with length k and perform several smaller computations in series. In order to have completeness of SNRs, each of these segments must overlap with the previous

one at the neighboring N data points. Then the computation time becomes $\mathcal{O}(\frac{k}{k-N}L(\log k)^2)$. The optimal length k depends on the template length which is given by the equation $N = \frac{2k}{\ln k + 2}$. This optimization scheme decreases the total computation time generally to $\mathcal{O}(L(\log N)^2)$. The precise optimization does not affect the asymptotic scaling. For example, with the choices of $k = 2N$ or $k = 3N$, it becomes $\mathcal{O}(2L(\log 2N)^2)$ or $\mathcal{O}(1.5L(\log 3N)^2)$ respectively, both being equivalent to $\mathcal{O}(L(\log N)^2)$.

The whole algorithm can be implemented on quantum and classical hardware and can be seen as a integral transform/convolution gate. The complete circuit is shown in Fig. 2 for a generic kernel. A similar hybrid construction of the swap test [18, 19], which computes the inner product of two vectors, with the purpose of simplifying the original quantum circuit with classical additions exists in Ref. [15], which we were inspired from. We also note that if shallower amplitude encoding algorithms are invented in the future, which were theoretically proven to exist [20], our method's total time complexity can be further reduced down to $\mathcal{O}(L(\log N))$.

3 Results

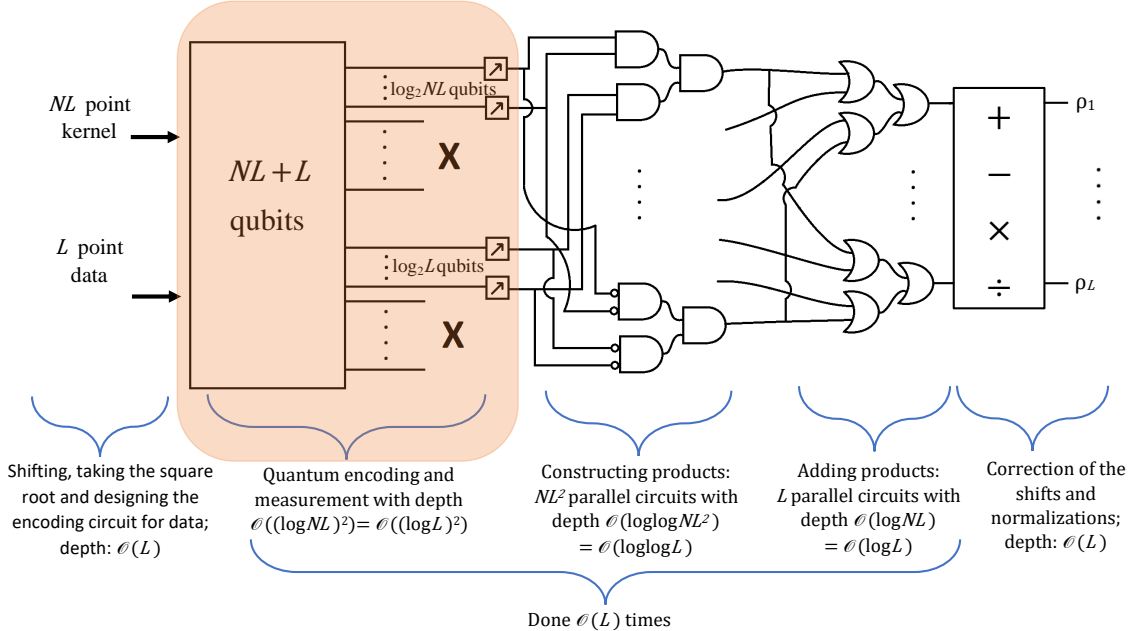
We experimentally demonstrate our method by accessing IBM Quantum systems through the cloud via Qiskit [21]. We computed the SNR time series of the astrophysical gravitational-wave event GW190521 [22] for a binary black hole merger gravitational waveform and demonstrate the accuracy of our method by comparing this result with the classical computation. We also did a preliminary study on artificial random data. IBM Quantum backends consist of fixed-frequency superconducting transmons [23] coupled by transmission line “bus” resonators arranged in a heavy-hexagonal lattice [24]. Single-qubit gates are achieved by on-resonant microwave drives at the ground-to-excited transition frequencies of the transmons, which vary due to the amorphous oxide of the single Josephson junction that forms the inductive part of the transmon (large superconducting pads form the geometric shunting capacitor of the analogous anharmonic oscillator). The cross-resonance entangling gate [25, 26] uses these variations in frequency to create a microwave-activated drive that entan-

gles coupled transmons and forms the basis of the CNOT gate. Measurement is done in the dispersive regime of circuit quantum electrodynamics [27, 28], in which a readout resonator is populated by photons far detuned from the qubit frequency, which dephase each qubit and imparts a state-dependent phase shift on the measurement pulse. The available native basis gates on these backends are highly-calibrated $\pi/2$ rotations `sx` gates, virtual-Z [29] `rz` gates for single qubit operations; and CNOT `cx` gates for multi-qubit operations. The other multi-qubit operations are executed with a combination of these gates. Sources of error in these operations are available [30] and show the main sources of error to be the CNOT error (average of 1%) and readout assignment error (1-4%). As deeper quantum circuits tend to have more CNOTs, these tend to be the biggest source of error. Due to limited physical connectivity, SWAP gates (consisting of 3 CNOTs) are particularly costly when mapping algorithms to current noisy quantum hardware.

Due to these limitations, we non-optimally divided the GW data into segments of length $k_d = 4$ and the template into segments of length $k_t = 2$. For the artificial random data, we created random data and a template with these sizes as well. The main obstacle for not using more data points at once is the significantly greater estimated error in the encoding when data is encoded to more than 2 qubits with the divide and conquer algorithm [17], due to the need of controlled SWAP operations between non-connected qubits. The signal lengths (=2) were chosen less than the data lengths (=4) in order to have more than one SNR value calculated with the described method. In this case there are 3 SNR values calculated per one data set. They correspond to the measurement probabilities of the template (x) and data (y) qubit probabilities $P(|0\rangle_x|00\rangle_y) + P(|1\rangle_x|01\rangle_y)$, $P(|0\rangle_x|01\rangle_y) + P(|1\rangle_x|10\rangle_y)$ and $P(|0\rangle_x|10\rangle_y) + P(|1\rangle_x|11\rangle_y)$.

3.1 Verification with artificial random data

The experiments we show here were ran on the backend `ibmq_lima`. The estimated total CNOT error probability and the total measurement error probabilities were both about 7% which are the main estimated sources of error. We have cho-



set the 2 point signal template arbitrarily as [2, 1]. Each data set of 4 numbers were chosen randomly from a normal distribution of zero mean and unit variance. In order to have all of the possible 8 measurement outcomes, the signal and data were arbitrarily shifted 0.1 more than their minimum negative values, i.e. $\Delta x = -\min(x_i) + 0.1$, $\Delta y = -\min(y_i) + 0.1$. Here we show results from 100 different data sets for each 2×10^4 measurements (shots) were made. Fig. 3 shows an example circuit from our experiment for the encoding of 3 qubits and their measurements. Qubits q1, q2, and q3 are used for encoding the data into the qubits q1 and q2. The signal template is encoded to q4.

Fig. 4 shows two scatter plots, one for the calculated $100 \times 3 = 300$ SNRs with quantum measurements vs. the true SNR values and one for the SNR errors between them vs. the true SNRs. The correlation coefficient for the points in the left figure was found to be 0.99, which should have been 1 ideally, and in the right figure as -0.57. The anti-correlation between the errors and the true SNR is

a clear indication that the errors have arisen due to the noise in the circuit. This is due to the fact that in order to have an SNR with a high magnitude, either the amplitude of the data should be high or more relevantly the relative amplitudes of the consequent data points need to have specific values. Any noise in the system can corrupt such delicate data segments. These corruptions increase the marginal entropies of encoded signal and data incoherently resulting in decrease in their mutual information. Low SNR points on the contrary do not get affected by such corruptions as their already low mutual information cannot decrease more. Another observation that can be made is the affinity to having positive SNR errors. This can be explained by the asymmetry in the encoding due to shifting to the positive values. Without the correction in Eq. (9), only the positive SNR values can be obtained. Therefore there is a fundamental lower limit on the SNR errors during the encoding. The effect of this lower limit is seen as having mostly positive SNR errors, especially for data segments

which have true negative SNR since their SNR values without the correction are the closest to zero. In Fig. 5 we show the result of a noise-free ideal quantum simulation with the same data and signal. The error in this case is only due to the Poisson errors due to finite number of measurements. The correlation coefficient between the SNRs is 1.0 and between the errors and the true SNRs is -0.1.

3.2 Analysis of the real gravitational-wave data

For our demonstration with the real gravitational-wave data, we have specifically chosen the event GW190521 [22]. It consists of relatively low gravitational-wave frequencies as it is one of the heaviest stellar-mass binary black hole systems ever detected by LIGO Scientific Collaboration and Virgo Collaboration [31, 32, 33, 34]. This allows us to down-sample the detected data series to reduce the data points to be processed with the quantum hardware. We used the 32 s long aLIGO Livingston [35] detector’s data sampled at 4 kHz¹. We down-sampled it to 200 Hz, after digitally applying an ideal low-pass filter with the cut-off frequency 99.98 Hz which is above the maximum frequency in the reconstructed astrophysical gravitational-wave. The noise power spectral density was found from the original data with Welch’s average periodogram method [36] with segment lengths of 512, using the MATPLOTLIB [37] python package’s MATPLOTLIB.PYTHON.PSD function. According to the estimation of the source properties of the gravitational-wave event at the detector frame [38]; the template waveform was generated at 200 Hz sampling with the GWSURROGATE [39] package with the NRSur7dq4 waveforms [40]. The used inputs were 154.7 solar masses and 120.1 solar masses for the black hole masses, (0.69,0,0) and (0,0.73,0) for the dimensionless spin vectors, and 12 Hz for the start frequency. With these configurations the SNRs were calculated for the data points starting at the UTC time 1242442967.15 for the consequent 0.45 s. The experiments were ran on the backend *ibmq_guadalupe*. In each run, from the 16 qubits on the backend, up to 10 qubits were used for independently encoding 3 partial data sets with

¹<https://www.gw-openscience.org/eventapi/html/GWTC-2/GW190521/>

3 qubits each and a template part with 1 qubit in parallel. The photo of the Falcon chip, which is the model of *ibmq_guadalupe*, and the layout of *ibmq_guadalupe* with the used qubits are shown in Fig. 6. At the time of execution, the CNOT error probabilities of each qubit connection and readout error probabilities of the qubits were all about 1%. The SNR for a particular time was found by adding the SNRs of the 2 point partial templates, which overlap with the previous and next partial template at 1 point.

The SNR series obtained with the quantum processor along with the pure classical computation are shown in Fig. 7. They were scaled such that the classically computed maximum SNR reaches the value of 1. The hybrid calculation shows high accuracy. The main observed errors are the decrease in the absolute values of very high and very low SNR values which shows the effect of the non-idealities of the current hardware, similar to our findings with artificial data. This shows that current quantum hardware can be used for performing calculations with comparable accuracy to a classical computer for practically relevant problems. With technological improvements, these calculations can be performed faster with quantum computers. The reasons why quantum advantage could not be achieved at this point are the CNOT error rates and the limited connectivity between the qubits which increases the required number of CNOT gates for encoding. These prohibit the construction of more intricate configurations for encoding larger number of qubits, which could have advantage over classical computation. With the improvements in the hardware, a useful application of this method can be executed in the future.

4 General applicability of the method

We point out that the described method for matched filtering can be straightforwardly generalized for any integral transform with a time dependent kernel by encoding a larger kernel of size $\sim NL$ instead of N . Due to logarithmic scalings in the repeated part of the algorithm, this generalization only increases the required qubit number and parallel gate counts according to $N \rightarrow NL$

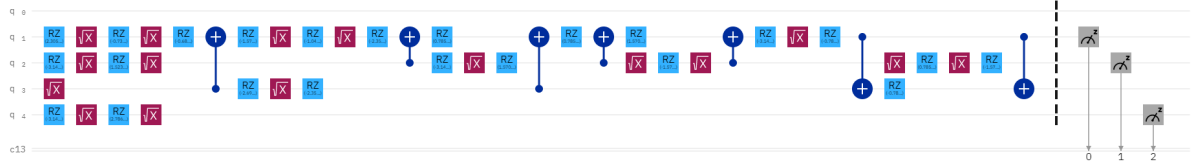


Figure 3: One of the circuits ran in the experiments for encoding

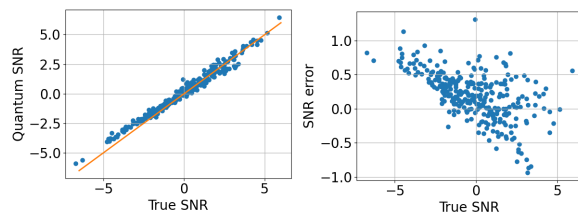


Figure 4: Results of the experiments on the quantum backend *ibmq_lima*: Left figure shows a scatter of the 300 SNRs computed with the use of qubits vs the true SNRs. The orange line is $x=y$ just for reference. Right figure shows the dependency on the errors in the computation on the true SNRs.

while keeping the time complexity constant, given the encoding circuit for the kernel was computed beforehand. Fig. 2 was drawn for a generic kernel. N in the sums and the length optimization remain the same. Calculations involving multi-dimensional functions, e.g. in image processing, obey the same scaling, where N and L represent the total number of points in the higher dimensional spaces, since any higher dimensional finite number of samples can be represented in one dimensional series. A corresponding one dimensional integral transform can be found according to the rasterizing scheme to one dimension. Last but not least, our method can be generalized to integral transforms having more than one input or more than one instances of the same input as in non-linear systems, Volterra series or coherent matched filtering of multi-detector data. In this case, the preprocessing for the encoding of the new inputs will naturally increase linearly with the total input count. Due to the same logarithmic scaling reason mentioned above, the scaling of this computation remains the same too while the qubit and gate counts increase. Our method uses quantum and classical computation complementarily instead of relying completely on quantum computation. This makes it more resilient to the typical gate errors due to having shallow quantum circuits and hence makes it a method that can be used reliably in the nearest future compared to the methods that require deeper quantum circuits. Improvements on wide range of applications from fundamental science to finance can be possible with our method, which we proved its viability on IBM Quantum’s hardware and which can have a quantum advantage with improving technology, especially with fully connected qubit networks.

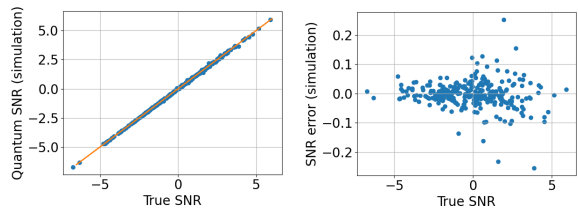


Figure 5: Results from an ideal noise free quantum simulation. The orange line is again $x=y$ just for reference. The only source of error is the Poisson uncertainty due to finite number of shots= 2×10^4 .

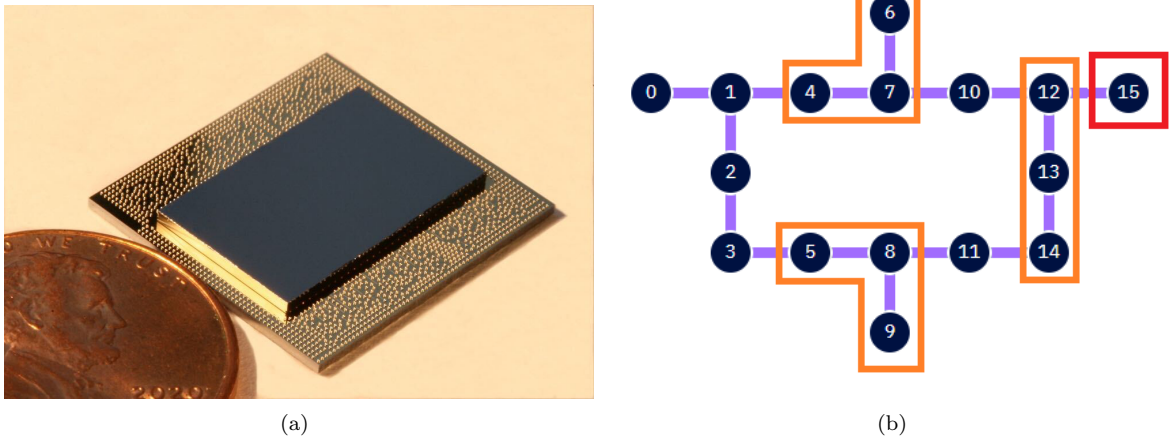


Figure 6: (a) Photo of the Falcon chip, the model of *ibmq_guadalupe* , next to a US penny (credit: IBM Research); (b) the qubit layout of the *ibmq_guadalupe*. The qubits we used for encoding the data are encapsulated with orange lines and the qubit we used for encoding the signal template is encapsulated with red lines. These qubits were chosen due to the lowest CNOT and readout error rates at the time of execution.

Acknowledgments

This document was reviewed by LIGO Scientific Collaboration under the document number P2200255. Authors are grateful to Mesut Çalışkan for this review, detailed inspection and helpful comments. Authors thank Columbia University in the City of New York for its unwavering and generous support. D.V. thanks Baran Bodur for suggesting the name convolution gate. D.V. was partially supported by European Research Council (ERC) under the European Union’s Horizon 2020 research and innovation programme grant agreement No 801781. C.T. is supported in part by the Helmholtz Association - “Innopool Project Variational Quantum Computer Simulations (VQCS)”. I.B. acknowledges the support of the National Science Foundation under grants PHY-1911796 and PHY-2110060, and the Alfred P. Sloan Foundation. We acknowledge the use of IBM Quantum services for this work. The views expressed are those of the authors, and do not reflect the official policy or position of IBM or the IBM Quantum team. This research has made use of data or software obtained from the Gravitational Wave Open Science Center (gw-openscience.org) [41], a service of LIGO Laboratory, the LIGO Scientific Collabora-

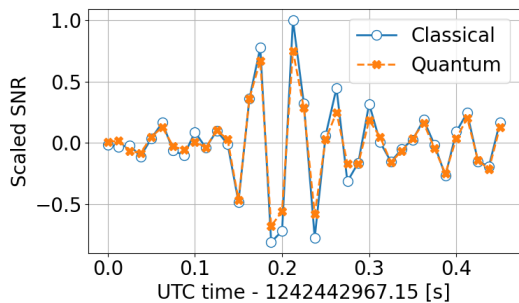


Figure 7: Scaled SNR time series around the gravitational-wave event from black hole merger GW190521. Blue circles show the classical result and orange crosses show the results obtained with the hybrid algorithm.

tion, the Virgo Collaboration, and KAGRA. LIGO Laboratory and Advanced LIGO are funded by the United States National Science Foundation (NSF) as well as the Science and Technology Facilities Council (STFC) of the United Kingdom, the Max-Planck-Society (MPS), and the State of Niedersachsen/Germany for support of the construction of Advanced LIGO and construction and operation of the GEO600 detector. Additional support for Advanced LIGO was provided by the Australian Research Council. Virgo is funded, through the European Gravitational Observatory (EGO), by the French Centre National de Recherche Scientifique (CNRS), the Italian Istituto Nazionale di Fisica Nucleare (INFN) and the Dutch Nikhef, with contributions by institutions from Belgium, Germany, Greece, Hungary, Ireland, Japan, Monaco, Poland, Portugal, Spain. The construction and operation of KAGRA are funded by Ministry of Education, Culture, Sports, Science and Technology (MEXT), and Japan Society for the Promotion of Science (JSPS), National Research Foundation (NRF) and Ministry of Science and ICT (MSIT) in Korea, Academia Sinica (AS) and the Ministry of Science and Technology (MoST) in Taiwan.

Data Availability

The datasets generated during and/or analyzed during the current study are available from the corresponding author on reasonable request.

Author contributions

D.V. and S.M. conceived the first conceptual idea. D.V. invented and developed the method, designed and executed the experiments, prepared the figures, and wrote the manuscript with inputs from all authors. D.V., I.B. and S.M. conceived the general applicability of the method. C.T. ran simulations and experiments for initial studies. M.A., N.T.B. and O.T.L. advised on the usage of IBM's hardware. I.B., Z.M. and S.W. provided additional discussions. S.M. oversaw the development of the idea. All authors contributed to the writing of the manuscript.

Competing interests

The authors declare no competing interests.

References

- [1] O. E. Neugebauer, *The Exact Sciences in Antiquity*. Princeton University Press, 1952.
- [2] J. B. J. Fourier, “Mémoire sur la propagation de la chaleur dans les corps solides,” *Nouveau Bulletin des Sciences par la Société Philomathique*, vol. 1, no. 6, pp. 112–116, 1808.
- [3] J. B. J. Fourier, *Théorie analytique de la chaleur*. F. Didot, 1822.
- [4] L. Debnath and D. Bhatta, *Integral Transforms and Their Applications*. Chapman and Hall/CRC, 2nd ed., 2006.
- [5] A. Oppenheim, A. Willsky, I. Young, and H. Nawad, *Signals and Systems*. Prentice-Hall signal processing series, Prentice-Hall, 1983.
- [6] School of Mathematics, Statistics and Actuarial Science, University of Kent, “Lecture notes on risk theory,” February 2010.
- [7] A. L. Fitzpatrick, J. Kaplan, J. Penedones, S. Raju, and B. C. van Rees, “A natural language for AdS/CFT correlators,” *Journal of High Energy Physics*, vol. 2011, nov 2011.
- [8] A. L. Fitzpatrick and J. Kaplan, “Unitarity and the holographic s-matrix,” *Journal of High Energy Physics*, vol. 2012, oct 2012.
- [9] W. Verhelst and P. Nilens, “A modified-superposition speech synthesizer and its applications,” in *ICASSP '86. IEEE International Conference on Acoustics, Speech, and Signal Processing*, vol. 11, pp. 2007–2010, 1986.
- [10] L. W. Couch, *Digital and Analog Communication Systems*, ch. 6-8. Pearson, 8th ed., 2012.
- [11] P. WOODWARD, “5 - simple theory of radar reception,” in *Probability and Information Theory with Applications to Radar (Second Edition)* (P. WOODWARD, ed.), International Series of Monographs on Electronics and Instrumentation, pp. 81–99, Pergamon, second edition ed., 1953.

[12] B. Allen, W. G. Anderson, P. R. Brady, D. A. Brown, and J. D. E. Creighton, “Findchirp: An algorithm for detection of gravitational waves from inspiraling compact binaries,” *Physical Review D*, vol. 85, Jun 2012.

[13] B. P. Abbott, R. Abbott, T. D. Abbott, M. R. Abernathy, F. Acernese, K. Ackley, C. Adams, T. Adams, P. Addesso, R. X. Adhikari, *et al.*, “Observation of gravitational waves from a binary black hole merger,” *Phys. Rev. Lett.*, vol. 116, p. 061102, Feb 2016.

[14] C. A. Ryan, B. R. Johnson, J. M. Gambetta, J. M. Chow, M. P. da Silva, O. E. Dial, and T. A. Ohki, “Tomography via correlation of noisy measurement records,” *Physical Review A*, vol. 91, no. 2, p. 022118, 2015.

[15] L. Cincio, Y. Subaşı, A. T. Sornborger, and P. J. Coles, “Learning the quantum algorithm for state overlap,” *New Journal of Physics*, vol. 20, p. 113022, nov 2018.

[16] M. Karnaugh, “The map method for synthesis of combinational logic circuits,” *Transactions of the American Institute of Electrical Engineers, Part I: Communication and Electronics*, vol. 72, no. 5, pp. 593–599, 1953.

[17] I. F. Araujo, D. K. Park, F. Petruccione, and A. J. da Silva, “A divide-and-conquer algorithm for quantum state preparation,” *Scientific Reports*, vol. 11, mar 2021.

[18] H. Buhrman, R. Cleve, J. Watrous, and R. de Wolf, “Quantum fingerprinting,” *Phys. Rev. Lett.*, vol. 87, p. 167902, Sep 2001.

[19] M.-S. Kang, J. Heo, S.-G. Choi, S. Moon, and S.-W. Han, “Implementation of swap test for two unknown states in photons via cross-kerr nonlinearities under decoherence effect,” *Scientific reports*, vol. 9, no. 1, pp. 1–14, 2019.

[20] X.-M. Zhang, T. Li, and X. Yuan, “Quantum state preparation with optimal circuit depth: Implementations and applications,” 2022.

[21] M. Treinish, J. Gambetta, P. Nation, P. Kassebaum, qiskit bot, D. M. Rodríguez, S. d. I. P. González, S. Hu, K. Krsulich, L. Zdanski, J. Garrison, J. Yu, J. Gacon, D. McKay, J. Gomez, L. Capelluto, Travis-S-IBM, M. Marques, A. Panigrahi, J. Lishman, lerongil, R. I. Rahman, S. Wood, L. Bello, T. Itoko, D. Singh, Drew, E. Arbel, J. Schwarm, and J. Daniel, “Qiskit: An Open-source Framework for Quantum Computing,” 2022.

[22] R. Abbott, T. D. Abbott, S. Abraham, F. Acernese, K. Ackley, C. Adams, R. X. Adhikari, *et al.*, “Gw190521: A binary black hole merger with a total mass of $150 M_{\odot}$,” *Phys. Rev. Lett.*, vol. 125, p. 101102, Sep 2020.

[23] J. Koch, T. M. Yu, J. M. Gambetta, A. A. Houck, D. I. Schuster, J. Majer, A. Blais, M. H. Devoret, S. M. Girvin, and R. J. Schoelkopf, “Charge-insensitive qubit design derived from the Cooper pair box,” *Physical Review A*, vol. 76, p. 042319, oct 2007.

[24] C. Chamberland, G. Zhu, T. J. Yoder, J. B. Hertzberg, and A. W. Cross, “Topological and subsystem codes on low-degree graphs with flag qubits,” *Physical Review X*, vol. 10, no. 1, pp. 1–21, 2019.

[25] J. M. Chow, A. D. Córcoles, J. M. Gambetta, C. Rigetti, B. R. Johnson, J. A. Smolin, J. R. Rozen, G. A. Keefe, M. B. Rothwell, M. B. Ketchen, and M. Steffen, “Simple All-Microwave Entangling Gate for Fixed-Frequency Superconducting Qubits,” *Physical Review Letters*, vol. 107, p. 080502, aug 2011.

[26] S. Sheldon, E. Magesan, J. M. Chow, and J. M. Gambetta, “Procedure for systematically tuning up cross-talk in the cross-resonance gate,” *Physical Review A*, vol. 93, p. 060302, jun 2016.

[27] A. Blais, R.-S. Huang, A. Wallraff, S. M. Girvin, and R. J. Schoelkopf, “Cavity quantum electrodynamics for superconducting electrical circuits: An architecture for quantum computation,” *Physical Review A*, vol. 69, jun 2004.

[28] A. Wallraff, D. I. Schuster, A. Blais, L. Frunzio, J. Majer, S. Kumar, S. M. Girvin, R. J. Schoelkopf, and R.-S. R.-S. Huang, “Strong

coupling of a single photon to a superconducting qubit using circuit quantum electrodynamics.,” *Nature*, vol. 431, pp. 162–7, sep 2004.

[29] D. C. McKay, C. J. Wood, S. Sheldon, J. M. Chow, and J. M. Gambetta, “Efficient Z gates for quantum computing,” *Physical Review A*, vol. 96, no. 2, pp. 1–8, 2017.

[30] “IBM Quantum Compute Resources.” <https://quantum-computing.ibm.com/services/resources?tab=systems>.

[31] B. Abbott, R. Abbott, T. Abbott, S. Abraham, F. Acernese, K. Ackley, C. Adams, R. Adhikari, V. Adya, C. Affeldt, *et al.*, “GWTC-1: A gravitational-wave transient catalog of compact binary mergers observed by LIGO and virgo during the first and second observing runs,” *Physical Review X*, vol. 9, sep 2019.

[32] R. Abbott, T. Abbott, S. Abraham, F. Acernese, K. Ackley, A. Adams, C. Adams, R. Adhikari, V. Adya, C. Affeldt, M. Agathos, K. Agatsuma, N. Aggarwal, O. Aguiar, L. Aiello, A. Ain, P. Ajith, S. Akcay, G. Allen, A. Allocata, P. Altin, A. Amato, S. Anand, *et al.*, “GWTC-2: Compact binary coalescences observed by LIGO and virgo during the first half of the third observing run,” *Physical Review X*, vol. 11, jun 2021.

[33] The LIGO Scientific Collaboration, The Virgo Collaboration, R. Abbott, T. D. Abbott, F. Acernese, K. Ackley, C. Adams, N. Adhikari, R. X. Adhikari, V. B. Adya, C. Affeldt, D. Agarwal, M. Agathos, K. Agatsuma, *et al.*, “Gwtc-2.1: Deep extended catalog of compact binary coalescences observed by ligo and virgo during the first half of the third observing run,” 2021.

[34] The LIGO Scientific Collaboration, The Virgo Collaboration, The KAGRA Collaboration, R. Abbott, T. D. Abbott, F. Acernese, K. Ackley, C. Adams, N. Adhikari, R. X. Adhikari, V. B. Adya, C. Affeldt, D. Agarwal, M. Agathos, K. Agatsuma, *et al.*, “Gwtc-3: Compact binary coalescences observed by ligo and virgo during the second part of the third observing run,” 2021.

[35] J. Aasi, B. P. Abbott, R. Abbott, T. Abbott, M. R. Abernathy, K. Ackley, C. Adams, T. Adams, P. Addesso, R. X. Adhikari, *et al.*, “Advanced LIGO,” *Classical and Quantum Gravity*, vol. 32, p. 074001, mar 2015.

[36] P. Welch, “The use of fast fourier transform for the estimation of power spectra: A method based on time averaging over short, modified periodograms,” *IEEE Transactions on Audio and Electroacoustics*, vol. 15, no. 2, pp. 70–73, 1967.

[37] J. D. Hunter, “Matplotlib: A 2d graphics environment,” *Computing in Science & Engineering*, vol. 9, no. 3, pp. 90–95, 2007.

[38] R. Abbott, T. D. Abbott, S. Abraham, F. Acernese, K. Ackley, *et al.*, “Properties and astrophysical implications of the $150 M_{\odot}$ binary black hole merger GW190521,” *The Astrophysical Journal*, vol. 900, p. L13, sep 2020.

[39] S. E. Field, C. R. Galley, J. S. Hesthaven, J. Kaye, and M. Tiglio, “Fast prediction and evaluation of gravitational waveforms using surrogate models,” *Phys. Rev. X*, vol. 4, p. 031006, Jul 2014.

[40] V. Varma, S. E. Field, M. A. Scheel, J. Blackman, D. Gerosa, L. C. Stein, L. E. Kidder, and H. P. Pfeiffer, “Surrogate models for precessing binary black hole simulations with unequal masses,” *Physical Review Research*, vol. 1, p. 033015, Oct. 2019.

[41] R. Abbott, T. D. Abbott, S. Abraham, F. Acernese, K. Ackley, C. Adams, R. X. Adhikari, V. B. Adya, C. Affeldt, M. Agathos, K. Agatsuma, N. Aggarwal, O. D. Aguiar, *et al.*, “Open data from the first and second observing runs of advanced ligo and advanced virgo,” *SoftwareX*, vol. 13, p. 100658, 2021.